Long-Tail Statistics of the Purcell Factor in Disordered Media Driven by Near-Field Interactions

R. Sapienza,[1,*] P. Bondareff,[1] R. Pierrat,[2] B. Habert,[1] R. Carminati,[2] and N. F. van Hulst[1,3]

[1]*ICFO-Institut de Ciencies Fotoniques, Mediterranean Technology Park, 08860 Castelldefels (Barcelona), Spain*

[2]*Institut Langevin, ESPCI ParisTech, CNRS, 10 rue Vauquelin, 75231 Paris, France*

[3]*ICREA-Institució Catalana de Recerca i Estudis Avançats, 08015 Barcelona, Spain*

(Received 22 December 2010; revised manuscript received 23 March 2011; published 20 April 2011)

In this Letter, we study the Purcell effect in a 3D disordered dielectric medium through fluorescence decay rates of nanosized light sources. We report distributions of Purcell factor with non-Gaussian long-tailed statistics and an enhancement of up to 8 times the average value. We attribute this large enhancement to strong fluctuations of the local density of states induced by near-field scattering sustained by more than one particle. Our findings go beyond standard diagrammatic and single-scattering models and can be explained only by taking into account the full near-field interaction.

DOI: 10.1103/PhysRevLett.106.163902 PACS numbers: 42.25.Dd, 33.50.−j, 42.50.Ct, 78.67.Bf

The ability to control the interaction between light and matter is the essence of many research disciplines including quantum information, energy harvesting, and sensing. This can be achieved by placing a light emitter in a localized optical mode and by exploiting the Purcell enhancement, an increase of spontaneous emission probability due to increased mode coupling [1]. The Purcell factor is a direct measure of the change in the local density of states (LDOS). This fundamental quantity drives spontaneous emission and macroscopic light transport properties [2].

Rich LDOS patterns, which strongly fluctuate in space, are expected in disordered complex media, due to mesoscopic fluctuations of the underlying mode structure. The latter arise from multiple scattering and interference of both propagating and evanescent (or surface) waves leading to strong intensity variations (speckles) and coherent mesoscopic phenomena, such as enhanced backscattering or Anderson localization [3]. Contrary to intuition, coupling to these modes has proven to enhance both spontaneous emission of single-photon sources [4] and collective stimulated emission processes [5].

In 3D media, pioneering experiments on nanosized sources at the interface between glass and a disordered medium [6] have shown both an increase and a reduction of the LDOS. In other experiments with buried sources, fluctuations of the LDOS that could not be explained by diffusive models have been observed [7]. In addition, in 2D plasmonic films, LDOS fluctuations have been shown to carry information on the spatial extent of eigenmodes [8]. Instead, in 2D electronic systems, LDOS distributions develop an asymmetric long tail beyond the Gaussian profile upon increasing the scattering strength [9], even far from Anderson localization, as recently confirmed by scanning tunneling microscopy experiments on magnetic semiconductors [10].

Optical LDOS fluctuations in 3D random media have been calculated [11] and for infinite systems have been proved to be equal to the C_0 speckle correlation of the intensity emitted by a point source [12]. While both these quantities strongly depend on the local near-field environment of the source and are therefore nonuniversal [13], their fluctuations have been predicted to be, in a diffusive scalar approximation, equal to $\pi/k\ell$, a universal function of k, the light k vector, and ℓ, the mean free path [14]. The two contrasting pictures of locality and of universal fluctuations determined by a single length ℓ cannot be easily reconciled.

In this Letter, we report on the measurement of the statistics of Purcell factors in 3D disordered media which presents wide and long-tailed statistics. The largest Purcell enhancement we observe is 8.8 times larger than the average of the distribution and 10 standard deviations away from the maximum of the distribution. We explain this asymmetric and non-Gaussian distribution by taking into account the full near-field multiple scattering. Our findings indicate the nonuniversal character of the LDOS fluctuations and therefore of C_0.

We have measured the fluorescence dynamics of ~300 nanosized light sources randomly placed in a 3D disordered medium. The emitter is a polymer (polystyrene-divinilbenzene) bead of 24 nm nominal radius internally doped with red (580–640 nm) Firefly dye molecules (Duke Scientific). It contains around 10^2–10^3 molecules in a small volume: It is a very bright source needed to overcome the poor in- and outcoupling through the disordered medium and has a well-defined, orientation-independent, optical response. This source is placed inside a 3D disordered medium made of ZnO powders of refractive index $n = 2.0$, polydisperse with average size 140 ± 50 nm. The samples have been grown starting from a 5 wt% (weight-weight percentage) water suspension of ZnO with 10^{-6} wt% concentration of fluorescent beads, through vertical deposition as in Ref. [15]. This low concentration guarantees that the density of emitters in the final sample is small enough to allow for individual addressing. A scanning electron microscope image of the

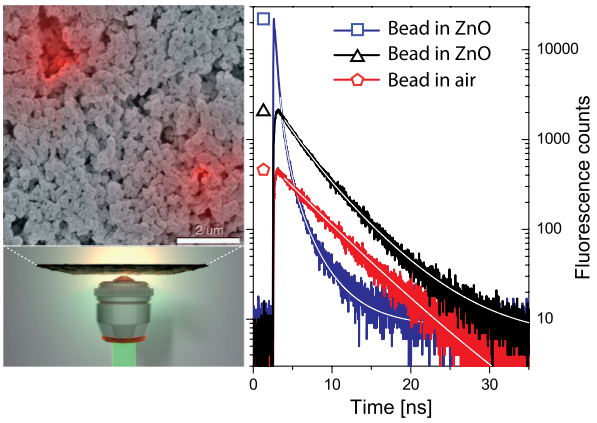

FIG. 1 (color online). Left panel: Schematic of the experiment showing a scanning electron microscopy image of the sample and the illumination or collection geometry. Right panel: Decay curves (colored lines) and their fit (white line) for different emitters, two different beads inside the ZnO disordered sample, and in air, on the glass surface.

obtained sample is shown in Fig. 1 (left panel). The grown ZnO samples have been optically characterized by the optical Ohm's law, $T \propto \ell/L$, as in Ref. [16]. The obtained transport mean free path is $\ell = 0.9 \pm 0.1$ μm at a wavelength of 600 nm, while the absorption length is $\ell_a = 30 \pm 10$ mm. These values turn into a $k\ell = 9.4$, much larger than unity. The transport time in the system, from any point to the detector, is much smaller ($\sim$ ps) than the fluorescence dynamics observed ($\sim$ ns).

The sample is illuminated with $\sim$50 ps pulsed laser light at 532 nm, 10 MHz repetition rate, and 0.1 mW of average power. This pump laser is focused at the sample front face through a 100$\times$ microscope objective with 1.4 numerical aperture. Because of the diffusive nature of the sample, the pump light illuminates a 90° wide conical section of the sample. The spontaneously emitted light of an illuminated bead is collected via the same microscope objective through dichroic and bandpass filters which ensure a detection window of 550–650 nm and a better than 10^{12} suppression of the pump laser.

The measurement is performed in two steps. (1) First, we locate an individual source by scanning the sample via wide-field microscopy. The source depth is assessed by measuring the size of the diffused light spot at the sample surface. (2) Second, we employ a confocal technique to direct the light emitted from the source to avalanche photodiodes. The fluorescence decay profile is reconstructed by time-correlated single-photon counting with an overall better than 100 ps response time. Raw data of three decay dynamics for emitters on glass and in a ZnO sample are shown in Fig. 1 (right panel). The reference decay of the source in air on glass is well fitted to a single-exponential decay, while inside the scattering medium a log-normal distribution of decay rates [17] accounts for the contribution of the many molecules at different positions inside the fluorescent bead.

The statistical analysis is obtained by repeating this procedure for many emitters in various samples at a depth larger than 3 μm in order to avoid surface effects. Figure 2 shows the histogram of the most-likely decay rate extracted from the fit for various samples. Figure 2(a) is the reference sample made of fluorescent beads at the interface between glass and air and between glass and a film of polyvinyl

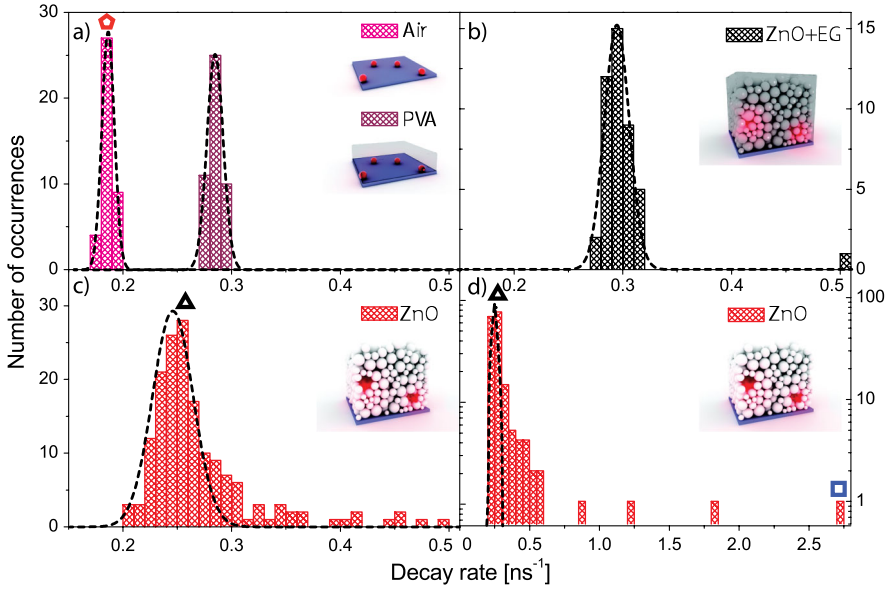

FIG. 2 (color online). Decay rates statistics for different experimental geometries (a) for beads on a glass-air and glass-PVA interface, (b) for beads in the ZnO + EG sample, and (c),(d) for beads in ZnO. Note that (d) is a zoom out of (c) in log scale that shows the asymmetric tail and several extremely high rates. The symbols identify the decay curve plotted in Fig. 1: The black triangle and the blue square identify a bead in the pure ZnO sample, while the red pentagon represents the bead in air on glass in Fig. 1.

alcohol (PVA) whose refractive index is 1.5. The reference shows a narrow distribution with a standard deviation of $3.0\% \pm 0.5\%$, for beads on glass, and $2.3\% \pm 0.3\%$, for the beads buried in a PVA film. The normalized variance $\mathrm{var}(\Gamma)/\langle\Gamma\rangle^2$ is 0.0009 and 0.0005, respectively. These narrow distributions and almost single-exponential decays (see Fig. 1, bead in air) are what one would expect from a bead with ~100 s of molecules inside [18].

Figure 2(b) represents the decay rate distribution measured for a weakly scattering medium made of ZnO powder in air by postdeposition addition of a drop of ethylene glycol (EG) ($n = 1.44$), which strongly decreases the dielectric contrast, thus increasing $k\ell$ to 24. The distribution obtained is wider than the reference case and shifted towards larger decays following the increased average refractive index. The standard deviation equals $0.033 \pm 0.005\ \mathrm{ns}^{-1}$, which is $11\% \pm 2\%$ of the mean; the normalized variance is $\mathrm{var}(\Gamma)/\langle\Gamma\rangle^2 = 0.012$.

Figures 2(c) and 2(d) are the main result of this Letter, as they show the decay rate distribution in a strongly scattering medium made of pure ZnO, for which the high contrast and scattering ($k\ell = 9.4$) induce a large fluctuation of decay rates observed. We observe a persistent fraction of ~20% of the beads which presents decays faster than $0.3\ \mathrm{ns}^{-1}$, more than expected from a simple Gaussian fit of the main peak below $0.3\ \mathrm{ns}^{-1}$, i.e., more than 5 times the half width at half maximum. Moreover, several extreme cases are observed such as the fast decay plotted in Fig. 1, with a $\Gamma = 2.8\ \mathrm{ns}^{-1}$, up to 8.8 times the average. The mean of the full long-tailed distribution of the most frequent decay rate is $0.31\ \mathrm{ns}^{-1}$, the maximum $0.25\ \mathrm{ns}^{-1}$, and the standard deviation $0.24 \pm 0.01\ \mathrm{ns}^{-1}$, which is $79\% \pm 4\%$ of the mean; the normalized variance is $\mathrm{var}(\Gamma)/\langle\Gamma\rangle^2 = 0.62$. When we compare our results to Ref. [7], we found that our data, when analyzed in the same range 0.2–0.55 ns^{-1}, gave a normalized variance of the average decay rate of 0.023 very similar to 0.020 as in Ref. [7]. We remark here that the log-normal fit to the decay curve is very satisfactory for all data.

We attribute the increased decay rates to Purcell enhancement and local optical properties, as proposed previously also in the context of (dielectric) amorphous polymer matrices [19]. Red emitting dyes (such as Firefly) have typically unitary quantum efficiency, and absorption in our ZnO powders is less than 2% (for a source depth less than 20 μm); therefore, we do exclude the possibility that the large lifetime changes result from fluctuations in the number of decay channels. Moreover, all particles show similar fluorescence intensity, which does not decrease with the higher rates, confirming the absence of competitive nonradiative channels. The normalized variance $\mathrm{var}(\Gamma)/\Gamma^2$ measured with values 0.012 for $\pi/k\ell = 0.12$ and 0.62 for $\pi/k\ell = 0.33$ does not scale like $\pi/k\ell$ as expected by a diagrammatic, scalar, and single-scattering model [12]; both the Purcell enhancements and thus the LDOS are not Gaussian-distributed.

In order to model numerically the qualitative behavior of the experimental decay rate statistics, we consider a system of radius R containing randomly distributed scatterers treated in the electric dipole approximation. The scatterers are described by their polarizability $\alpha(\omega) = -3\pi c^3\gamma/[\omega^3(\omega - \omega_0 + i\gamma/2)]$, where ω_0 is the resonance frequency, γ is the linewidth, and c is the speed of light in vacuum. The parameters ω_0 and γ are adjusted so that the scattering cross section corresponds to that of ZnO nanoparticles of size 140 nm at a wavelength $\lambda = 2\pi c/\omega = 610$ nm. The density of scatterers is chosen such that $k\ell = 9.4$. The emitter is placed at the center $\mathbf{r}_0$ of the sphere and is surrounded by an exclusion volume of radius $R_0 = 0.07\ \mu$m as shown in the inset in Fig. 3. Theoretically, in the weak coupling regime, the decay rate Γ averaged over the orientation of the emitting dipole is proportional to $\mathrm{Im}[\mathrm{Tr}\mathbf{G}(\mathbf{r}_0, \mathbf{r}_0, \omega_0)]$ [20]. $\mathbf{G}$ is the dyadic Green function and connects an electric dipole $\mathbf{p}$ at position $\mathbf{r}_0$ to the radiated electric field at position $\mathbf{r}$ through the relation $\mathbf{E}(\mathbf{r}) = \mu_0\omega_0^2\mathbf{G}(\mathbf{r}, \mathbf{r}_0, \omega_0)\mathbf{p}$. Numerically, the computation of the decay rate reduces to a coupled-dipole numerical computation [21] of the Green function of the system. Figure 3 shows the numerical distribution of the decay rate. In particular, we see that the long-tail behavior for large values of Γ is recovered.

In addition, thanks to the flexibility of the numerical method we can compute the LDOS distributions for systems with the same scattering strength but different microscopic properties. Figure 4 shows that the fluctuations of the decay rate can be strongly different in systems with the same value of $\pi/k\ell$ and different exclusion volume, showing that $k\ell$ cannot be considered as the single parameter driving the statistical distribution. Moreover, systems with the same exclusion volume give rise to similar values of C_0 and similar statistical line shapes, confirming the crucial role of near-field interactions at the scale of the exclusion volume, as predicted in Ref. [13].

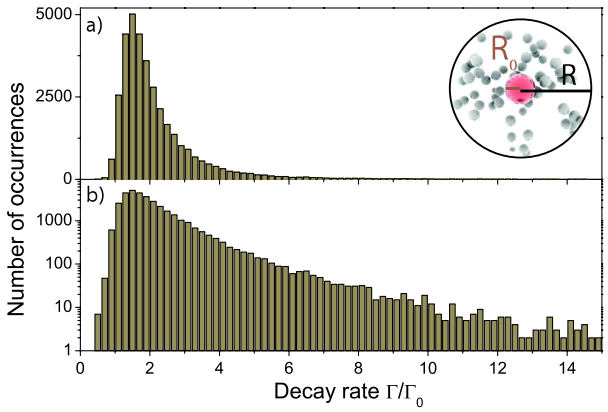

FIG. 3 (color online). Numerical distribution of the decay rate Γ for ZnO particles normalized by the decay rate in vacuum Γ_0 for $R_0 = 0.07\ \mu$m and $R = 1.25\ \mu$m. (b) is a logarithmic plot of (a). Inset: Schematic view of the system.

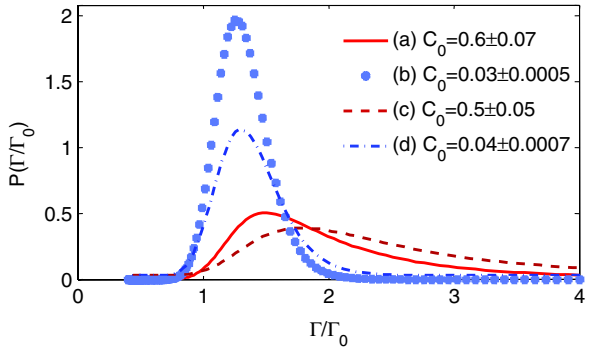

FIG. 4 (color online). Numerical distributions of the decay rate for four different systems with the same value $k\ell = 9.4$ and $R = 0.63$ μm. Curves (a) and (c) correspond to an excluded radius $R_0 = 0.07$ μm while (b) and (d) to $R_0 = 0.14$ μm. Curves (c) and (d) are the same as (a) and (b) but with a doubled density of scatterers.

We can attribute large values of the Purcell factor to rare events that create optical modes confined in a small volume around the source. While similar modes have been discussed in the context of random lasers [22], our analysis in terms of the Purcell factor suggest that these confined optical modes are sustained by near-field interactions between the emitters and the surrounding ZnO particles. As our simulations show, near-field interactions of a dipolar source with more than one particle can give rise to large LDOS values (Fig. 3), even for scattering events taking place on distances much smaller than the wavelength. These events are responsible for the high sensitivity of the LDOS on the *local* near-field environment (Fig. 4). Note, e.g., that the quasistatic (near-field) interaction of a dipole with a single flat ZnO surface can already change the LDOS value up to a factor n^4 [23].

In conclusion, we have studied the statistics of LDOS by the Purcell effect for nanosized emitters buried in a 3D random medium. Long-tailed and non-Gaussian behavior is evident, with large decay rates. This is not accounted for by the present analytical model, cannot be reduced to a single length like ℓ, and can be explained only by including the full near-field multiple-scattering contribution as we confirmed by numerical simulations. The nonuniversality of the LDOS distribution makes it a valuable quantity for sensing or imaging the microscopic structure of complex media. In contrast to ensemble methods, a single source approach can provide robust information on the photon scattering regime, the eventual scattering correlations, or the transition to Anderson localization.

We thank A. P. Mosk for fruitful discussions. This research was funded by the MICINN, programs FIS2009-08203, CONSOLIDER CSD2007-046, RyC, Fundació CELLEX, and the EU Project ERC and *Nanomagma* NMP3-SL-2008-214107.

*riccardo.sapienza@icfo.es

[1] E. M. Purcell, Phys. Rev. **69**, 674 (1946).
[2] A. Lagendijk and B. A. van Tiggelen, Phys. Rep. **270**, 143 (1996); R. Carminati and J. J. Sáenz, Phys. Rev. Lett. **102**, 093902 (2009); P. D. García *et al.*, Phys. Rev. B **79**, 241109 (2009).
[3] Y. Kuga and A. Ishimaru, J. Opt. Soc. Am. A **1**, 831 (1984); M. P. VanAlbada and A. Lagendijk, Phys. Rev. Lett. **55**, 2692 (1985); P. E. Wolf and G. Maret, Phys. Rev. Lett. **55**, 2696 (1985); S. John, Phys. Rev. Lett. **53**, 2169 (1984); P. W. Anderson, Philos. Mag. B **52**, 505 (1985); F. Scheffold and G. Maret, Phys. Rev. Lett. **81**, 5800 (1998).
[4] L. Sapienza *et al.*, Science **327**, 1352 (2010).
[5] S. Gottardo *et al.*, Nat. Photon. **2**, 429 (2008); D. S. Wiersma, Nature Phys. **4**, 359 (2008).
[6] P. V. Ruijgrok *et al.*, Opt. Express **18**, 6360 (2010).
[7] M. D. Birowosuto *et al.*, Phys. Rev. Lett. **105**, 013904 (2010).
[8] V. Krachmalnicoff *et al.*, Phys. Rev. Lett. **105**, 183901 (2010).
[9] I. V. Lerner, Phys. Lett. A **133**, 253 (1988); A. D. Mirlin, Phys. Rev. B **53**, 1186 (1996).
[10] A. Richardella *et al.*, Science **327**, 665 (2010).
[11] A. D. Mirlin, Phys. Rep. **326**, 259 (2000).
[12] B. A. van Tiggelen and S. E. Skipetrov, Phys. Rev. E **73**, 045601(R) (2006).
[13] L. S. Froufe-Pérez, R. Carminati, and J. J. Saenz, Phys. Rev. A **76**, 013835 (2007); A. Cazé, R. Pierrat, and R. Carminati, Phys. Rev. A **82**, 043823 (2010).
[14] B. Shapiro, Phys. Rev. Lett. **83**, 4733 (1999).
[15] P. D. García *et al.*, Adv. Mater. **19**, 2597 (2007).
[16] R. Sapienza *et al.*, Phys. Rev. Lett. **99**, 233902 (2007).
[17] I. S. Nikolaev *et al.*, Phys. Rev. B **75**, 115302 (2007).
[18] L. Novotny and B. Hecht, *Principles of Nano-optics* (Cambridge University Press, Cambridge, England, 2006).
[19] R. A. L. Vallée *et al.*, Chem. Phys. Chem. **6**, 81 (2005); R. A. L. Vallée *et al.*, Phys. Rev. Lett. **91**, 038301 (2003).
[20] J. M. Wylie and J. E. Sipe, Phys. Rev. A **30**, 1185 (1984).
[21] R. Pierrat and R. Carminati, Phys. Rev. A **81**, 063802 (2010).
[22] V. M. Apalkov, M. E. Raikh, and B. Shapiro, Phys. Rev. Lett. **89**, 016802 (2002); P. Sebbah *et al.*, Phys. Rev. Lett. **96**, 183902 (2006).
[23] K. H. Drexhage, J. Lumin. **1–2**, 693 (1970).